RSC Advances

ROYAL SOCIETY OF CHEMISTRY

www.rsc.org/advances

Graphene Oxide Wrapped Gold Nanorods for Enhanced Photothermal Stability

Qingli Wei, Hong Ni, Xue Jin and Jing Yuan[a]*

TOC

NanoGO wrapped Gold nanorods show enhanced photothermal stability under continuous NIR laser irradiation.

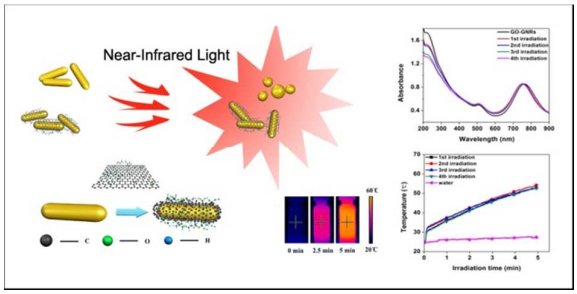

Journal Name

ARTICLE

Graphene Oxide Wrapped Gold Nanorods for Enhanced Photothermal Stability

Received 00th January 20xx,
Accepted 00th January 20xx

DOI: 10.1039/x0xx00000x

www.rsc.org/

Qingli Wei,[a] Hong Ni,[a] Xue Jin[b] and Jing Yuan[a]*

Nanocomposite of gold nanorods coated with nanosized graphene oxide (GO-GNRs) was fabricated in ammonium hydroxide solution and its photothermal stability was invesigated upon exposure to near-infrared (NIR) light irradiation. The optical property and morphology of the GO-GNRs nanohybrids retained unchanged after 4 repeated NIR exposu which is considerably stable compared with the as-synthesized gold nanorods. In addition, the GO-GNRs nanohybrids showed a superb reproducibility of photothermal performance and an excellent colloidal stability. Such graphene oxide modified gold nanorods with enhanced photothermal stability are well suited for further biological applications such as sensing, bioimaging and photothermal therapy.

Introduction

Laser illumination in the near infrared (NIR) region provides much deeper tissue penetration with minimal damage to surrounding healthy tissue in comparison to light in the UV and visible region. Nanoparticles, including gold nanoparticles in various shapes[1,2] and copper(II) sulfide nanocrystals[3], have distinctive surface-plasmon-resonance (SPR) properties in the NIR regions. The unique optical properties can be well utilized, due to the fact that when irradiated with NIR light, nanoparticles can generate heat to surrounding areas. The temperature increases could be adjusted through varying laser intensity, light duration, and the concentration of liquid samples. Therefore, the NIR light absorbing nanomaterials have been extensively investigated as photothermal agents which have been applied in drug delivery[4], cancer diagnosis and treatment[5], as well as sensors[6].

Gold nanorods (GNRs) have received significant attentions in the fields of material and life science due to their high extinction coefficient of longituditional surface plasmon (LSPR) in the NIR region. GNRs with different aspect ratios[7], can be controllably synthesized, which exhibit a tunable photothermal performance upon NIR laser irradiation. Therefore, these rod-like nanoparticles, with relative smaller size, are promising heat sources for the application of photothermal therapy (PTT)[8].

Despite the novel properties of GNRs, it's difficult to directly utilize them in the field of biomedical technology due to the high cytotoxicity and photothermal instability of the as-prepared GNRs. Cetyltrimethylammonium bromide (CTAB), as a stabilizing agent utilized in the synthesis of GNRs, is highly toxic to cells[9], which severely limits the biological applications of GNRs. Various approaches, such as ligand exchange[10, 11] or encapsulation[12] by nontoxic molecules, have been explored in an effort to reduce cytotoxicity of GNRs. Another significant concern is the photothermal stability of GNRs. Upon irradiation by NIR laser, the heat generated from the photothermal effect often melts GNRs into solid spheres which results in a poor photothermal stability and disappeared NIR-SPR properties[13]. There are many reports regarding the photothermal stability of untreated GNRs[14], GNRs ultrathin film[15], and GNRs coated with silica shells[16], PC[13] and polyelectrolytes[17] as well.

Graphene oxide (GO), an important graphene derivative, has attracted extensive interests in various areas such as catalysis[18] and hydrogen storage[19]. In particular, GO has potential applications in biomedicine as a good candidate for cellular imaging and drug delivery[20]. GO, a fairly safe material, provides minimal side effects and toxicity to cells in small doses[21]. In addition, it is well known that GO maintains well soluble in water due to the negative charge on the sheet surface. Such charge property can be utilized for surface modification of GNRs, as the surface of CTAB-capped GNRs (CTAB-GNRs) is positively charged. Through electrostatic interaction, CTAB-GNRs can be readily wrapped by a thin layer of GO to improve their biocompatibility. The composition of large GO sheets and GNRs has been previously studied[22]. However, there is an increasing requirement to investigate the properties of GNRs coated with nanosized GO (nanoGO) sheets instead of large ones[23] for further biomedical applications.

Here, we synthesized nanoGO-encapsulated GNRs (GO-GNRs). It was amazing to observe that the GO-GNRs didn't undergo distinct shape transformation, spectral change, and

[a]Department of Chemistry, Capital Normal University. 105 West 3rd Ring North Rd, Beijing, 100048, China. Email: jyuan@cnu.edu.cn
[b]Beijing National Laboratory for Molecular Science, CAS Key Laboratory of Colloid, Interface and Chemical Thermodynamics, Institute of Chemistry, Chinese Academy of Sciences, Beijing, 100190, China.
† Supplementary Information (ESI) available: See DOI: 10.1039/x0xx00000x

reduced photothermal performance after 785 nm NIR laser irradiation. The high photothermal stability we found in the GO-GNR nanocomposites is a significant characteristic for further biomedical applications such as photothermal therapy and NIR-triggered drug delivery system.

Experimental Section

Materials

Cetyltrimethylammoniumbromide (CTAB) (≥99%) was purchased from Sigma-Aldrich. Silver nitrate ($AgNO_3$) (99%) and Gold(III) chloride trihydrate ($HAuCl_4$) (49.0% Au) was purchased from J&K Reagent Company. L-ascorbic acid was purchased from the Biodee Reagent Company (Beijing, China). Sodium borohydride ($NaBH_4$) (96%) were purchased from Sinopharm Company. Graphene oxide (GO) (>99%) was purchased from JCNANO (Nanjing, China). All chemicals were used as received without further purification. Ultrapure water (18 MΩ) was used in all the experiments.

Synthesis of GNRs.

Seed Solution. Ice-colded $NaBH_4$ (0.60 mL, 0.010 M) was added into the mixture of 5.0 mL of 0.20 M CTAB and 5.0 mL of 0.50 mM $HAuCl_4$, which resulted in a brownish yellow solution. Vigorous stirring of the seed solution was continued for 2 min to remove excess reductant. After stirring, the seed was kept at 27 °C in a water bath for 2 h.

Growth Solution of GNRs. CTAB (5 mL, 0.20 M), $AgNO_3$ (200 uL of 0.0040 M), $HAuCl_4$ (5.0 mL of 1.0 mM) were mixed and stirred at 25 °C. L-ascorbic acid (1 mL, 0.10 M) was then added slowly to the mixture, and that solution became colorless immediately. The final step was the addition of 0.120 mL of the seed solution. The growth solution was placed in a water bath at 28±1 °C. The color of the solution gradually changed to amaranth within 10-20 min. The temperature of the growth medium was kept constant at 28±1°C for 10 hours.

The synthesized GNRs were centrifuged twice at 12000 rpm for 20 min to remove excess CTAB. After centrifugation, the precipitate was re-dispersed in ultrapure water. The concentration of the resulting samples was determined via UV-visible spectroscopy (the molar extinction coefficient of GNR solution is 4.6×10^9 M^{-1} cm^{-1})[24].

Preparation of nanosized graphene oxide (nanoGO). GO powder (10.0 mg) was dissolved in ammonium hydroxide (20 mL), and then exfoliated by using ultrasonic cell disruptor (90% amplitude, 800 W, 2.5 h) until the entire size distribution was below 120 nm. Centrifugation (22000 rpm, 20 min) was performed to remove the un-exfoliated large GO sheets. The prepared nanoGO showed a narrow size distribution of around 110 nm.

Fabrication of GO–GNRs.

Purified CTAB-stabilized GNR solution (10 mL, 0.2 nM) was dropped into nanoGO solution (20 mL, 0.5 mg/mL,) with a continuous stirring. After stirring for another 30 mins, the solution was centrifuged (12000 rpm, 15 min) twice to remove excess free GO nanosheets. Precipitates were collected and re-dispersed with 10 mL of water.

Characterization.

UV-visible spectra were collected on a Shimadzu UV-vis 2550 spectrophotometer. Both Zeta-potential and Dynamic light scattering (DLS) measurements were conducted with a Zetasizer Nano ZS90 (Malvern Instruments). Morphological features of the GNRs and GO–GNRs were characterized by Hitachi 7650 transmission electron microscopy (TEM). Raman samples were prepared on silicon slices, and dried under vacuum overnight at 25 °C. Raman spectra were measured using a RENISHAW inVia Raman Microscope using an excitation wavelength of 633 nm (50× objective, 50 mW). AFM images were obtained on a Dimension FastScan (Bruker), using the ScanAsyst mode under ambient conditions.

Photothermal experiments in solutions were conducted using a FLIR E40 thermal imaging system, which was described in a previous literature[25]. GO-GNRs and CTAB-GNRs solutions with the same concentration (0.19 nM) were irradiated by a 785 nm laser (Xi'an Sampling Laser Techinc Institute) and the temperature signals were recorded with FLIR tools systems.

Results and Discussion

The combination of nanoGO with GNRs was characterized by UV-visible spectroscopy (Figure 1A). CTAB-stabilized GNRs contain two special peaks including a strong Longitudinal Surface Plasmon Resonance (LSPR) in long-wavelength region (803 nm) and a weak transverse surface Plasmon oscillation in short-wavelength region (510 nm). The average aspect ratio of these GNRs is about 3.6, with a length of 38.7±4.1nm and a diameter of 10.7±1.1nm (Figure S1). After incorporation with nanoGO, the LSPR peak of GO-GNRs displayed a blue-shift from 803 nm to 760 nm, which indicated the possibility of a slightly reduced aspect ratio of GNRs after wrapped with GO nanosheets. No obvious broadening or dramatic shifting of the LSPR peak was observed, which provided strong evidence for the persistence of mono-dispersion as well as the shape of GNRs upon surface modification. This was further confirmed by the TEM images (Figure 1B). Moreover, the photothermal effect of GO-GNRs was not affected, which will be demonstrated later.

As shown in Figure 1C, the re-dispersed GO-GNRs solution (the middle one) appears to be uniform and much darker compared with the unmodified GNRs solution (the left one). The color change together with the increment of UV signal below 400 nm (blue curve in Figure 1A) strongly suggested the incorporation of GNRs with GO nanosheets. Although a small amount of GNRs were detected in supernatant after centrifugation (Figure 1A, black line), most of the incorporated GO-GNR nanocomposites could be segregated from the sample and regained in ultrapure water (Figure 1A, blue line). A thin layer of GO nanosheet tightly attached onto the surface of CTAB-GNRs through electrostatic interaction to modify the surface property and photothermal performance of GNRs.

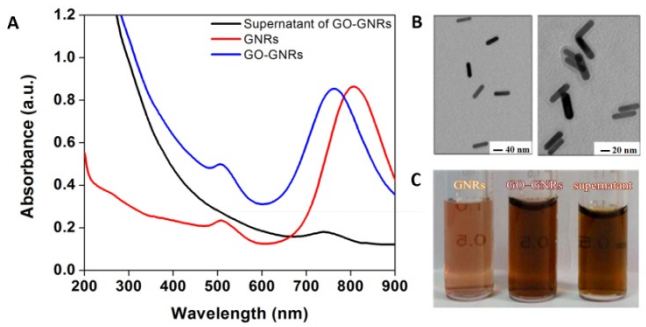

Figure 1. (A) UV-visible spectrum of GNRs (red line), GO-GNRs (blue line) and the supernatant of GO-GNRs after centrifugation (black line); (B) TEM images of GNRs (left) and GO-GNRs (right); (C) Digital photograph of the samples was arraied according to the above sequences.

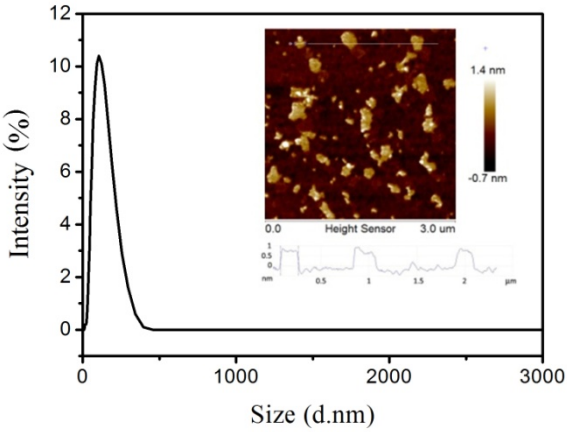

Figure 2. Size distribution of graphene oxide sheets in ammonium hydroxide solution after ultrasonication. The synthesized nanoGO sheets were approximate 110 nm. Insert: AFM image of exfoliated nanoGO sheets.

NanoGO was prepared through a method in which GO powders were dissolved in a certain amount of ammonium hydroxide solution (28 %, w/w) and exfoliated by an ultrasonic cell disrupter in an ice bath. Aggregation among layers of GO could be considerably prevented in the process of prolonged ultrasonic treatment under low temperature. NanoGO was collected from the supernatant after centrifugation at 22000 rpm for 20 min. Dynamic light scattering (DLS) measurements were performed with a Zetasizer Nano ZS90 instrument to analyze the particle distribution of the samples. The size of raw GO sheets was 2,500 ± 500 nm (Figure S2). After ultrasonic decomposition, the size of GO sheets was reduced to 110 ± 50 nm (Figure 2). AFM image showed that the thickness of the exfoliated nanoGO sheets was about 0.8~1.0 nm, confirming that a single-layer structure of GO sheets was obtained[26].

GO-GNRs nanocomposites were fabricated by adding GNR solution into nanoGO solution in a dropwise manner. The free standing nanoGO sheets preferred to stay in supernatant. Once incorporated with GNRs through electrostatic interaction, these nanoGO sheets could be pulled down together with GNRs during centrifugation. Consequently, GO-GNRs could be well separated from the free nanoGO by means of centrifugation.

Sample	nanoGO	CTAB-GNRs	GO-GNRs
Zeta potential (mV)	-18.1	25.5	-15.7

Table 1. The Zeta potential of nanoGO, CTAB-GNRs and GO-GNRs were measured in ultrapure water at 25 ℃.

Zeta potential measurements were performed to explore the efficiency of this surface modification. As shown in Table 1, the surface charges of pure nanoGO, CTAB-GNRs, and GO-GNRs were measured. CTAB-GNRs displayed a positive zeta potential which came from the positively charged CTAB bilayers packing on the surface of GNRs. The fabrication of GO-GNRs nanocomposites was achieved in a way that CTAB-stabilized GNRs interacted with negatively charged GO through electrostatic attraction. A corresponding decrease in zeta potential from +25.5 mV to -18.1 mV confirmed an efficient surface modification with negatively charged GO sheets. In addition, negative charges on the surface of GO-GNRs provided a mutual repulsion of these nanoparticles to ensure their monodispersity and colloidal stability.

DLS measurements provided further evidence for the combination between these two materials (Figure 3). The as-prepared CTAB-GNRs were centrifuged twice (12,000 rpm, 20 min) to remove excess CTAB, and the rod size was approximately 40 nm. Incorporation with GNRs resulted in a wider size distribution with an increase of approximate 100nm in size. After 2 centrifugations, the size distribution of re-dispersed GO-GNR solution decreased back to 105 ± 50 nm. Therefore we proposed that the observed peak broadening and increase in size for the sample before centrifugation came from the aggregation of nanoGO sheets, as free positively charged CTAB molecules in GNRs solution could interact with negatively charged nanoGO to reduce the electrostatic repulsion between those nanoGO sheets. The bulk nanoGO aggregates, which preferred to stay in supernatant, could be easily removed through centrifugation. Compared with nanoGO, the slight decrease in size for GO-GNRs might be ascribed to the deformation of nanoGO from flat sheet to curled shape. Monodispersity of GO-GNRs without any sign of shoulder peaks around 40 nm strongly indicated that nearly all the GNRs were wrapped by nanoGO sheets.

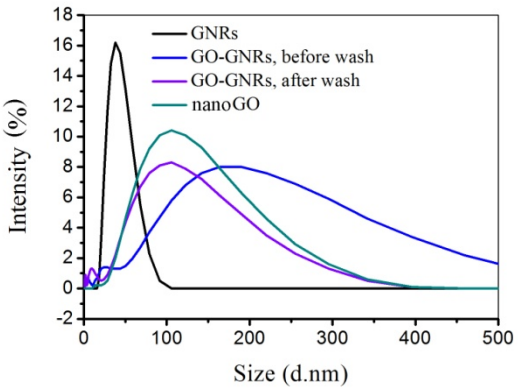

Figure 3. Size distribution of GNRs, GO-GNRs before centrifugation, GO-GNRs after centrifugation, and nanosized GO.

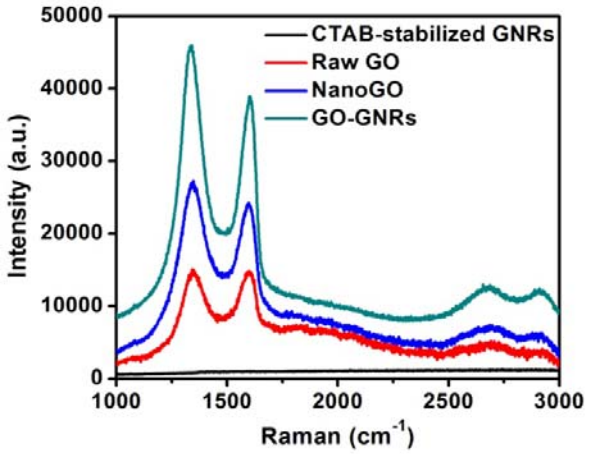

Figure 4. Raman spectra of CTAB-stabilized GNRs, raw GO, exfoliated nanoGO and GO-GNRs after washed twice.

Raman spectroscopy is a powerful tool to detect structural changes in carbon materials. Figure 4 shows the Raman spectra of CTAB-stabilized GNRs, raw GO, exfoliated nanoGO, and GO-GNR samples. As we expected, the CTAB-stabilized GNRs didn't show any signal in the detected region, while typical peaks around 1,341 cm^{-1} (D band) and 1,581 cm^{-1}(G band)[27] were observed for all GO-contained samples. The exfoliated nanoGO showed an increased D/G intensity ratio compared with raw GO, which might be attributed to a decrease of the sp^2 domains[28] and a possible chemical reduction of GO sheets[29] upon exfoliation. It is well-known that completely reduced GO sheets have poor colloidal stability in water due to their hydrophobicity[30]. The observed good colloidal stability in the GO-GNR nanocomposites suggested an incomplete reduction of nanoGO.

Figure 5 shows the photothermal performance of CTAB-GNR and GO-GNR solutions under NIR illumination (785 nm, continuous wave (CW)). Three different laser intensities were selected, which were 1.5 W/cm^2, 1.9 W/cm^2, and 2.3 W/cm^2. All sample solutions were adjusted to the same concentration (OD = 0.88) and 2 mL of each sample was illuminated for 5 mins, which resulted in a gradual increase in temperature. The temperature increased to 48.3 °C, 56.7 °C, and 62.4 °C for CTAB-GNR samples and to 48.4 °C, 54.5 °C, and 60.9 °C for GO-GNR samples after 5 min illumination in correspondence to different laser intensities at 1.5 W, 1.9 W and 2.3 W. Ultrapure water only increased in temperature by 1.3 °C after 5 min illumination at 2.3 W/cm^2, which confirmed that the majority of the photothermal effects came from NIR responsive nanoparticles.

After solutions were cooled down to room temperature, another three repeated irradiation processes were carried out to explore the stability of their photothermal performance. Obviously, CTAB-GNRs showed reduced photothermal performance under repeated irradiation, which was illustrated by the reduced slopes in the thermal curves (Figure 5 A, C, E). This phenomenon conformed with previous reports about the photothermal instability of CTAB-GNRs[14]. In addition, the slopes of these thermal curves decreased more dramatically when irradiated with higher laser intensities (Figure 5C, 5E). A collection of photos vividly displayed a poor photothermal performance of CTAB-stabilized GNRs after repeated laser irradiation (Figure 5G).

Significant difference in photothermal performance was observed for GO-GNR nanocomposites under the same repeated irradiation. Apparently, the thermal curves were extremely repeatable within 4 repeated experiments (Figure 5, B, D, F), which indicated an excellent stability in photothermal performance for GO-GNR nanocomposites. In addition, with a higher laser power at 2.3 W, the thermal curves slightly shifted upward under repeated irradiation, which might be attributed to the possible destruction of GO sheets by high intensity laser irradiation (Figure 5F). Four corresponding photo images of thermal effects were represented in Figure 5H, which illustrated the excellent photothermal stability of GO-GNRs.

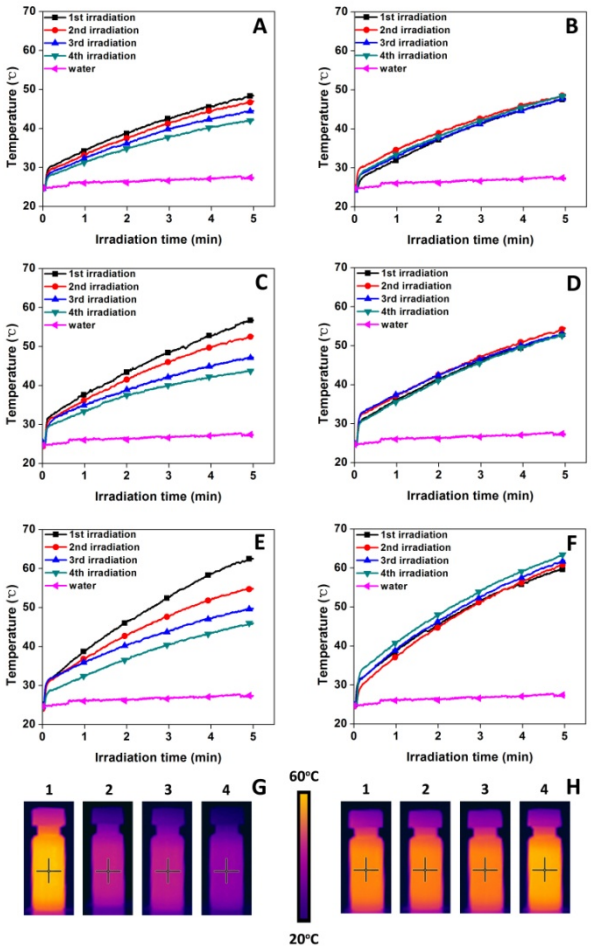

Figure 5. Photothermal curves of CTAB-GNRs (A, C, E) and GO-GNRs (B, D, F) under irradiation with 785 nm CW laser at different laser intensity (A, B: 1.5 W/cm^2, C, D: 1.9W/cm^2, and E, F: 2.3 W/cm^2) for 5 minutes. Ultrapure water showed a slight increase in temperature under irradiation at 2.3 W/cm^2(the pink curves). Digital imag of CTAB-GNRs (G) and GO-GNRs (H) in 4 corresponding repeated photothermal experiments.

UV-visible characterization is generally used to probe the shape stability and aggregation behaviour of GNRs. As shown in Figure 6A, CTAB-GNRs showed distinct spectral changes after NIR exposure even at the lowest laser intensity at 1.5 W/cm^2. The LSPR peak around 760 nm significantly decreased and became much broader after repeated irradiation. Further increase of laser intensity to 1.9 W and 2.3 W led to a significant decrease in LSPR intensity and an obvious blue-shift of the peak positions (Figure 6, C, E), which indicated a decreased aspect ratio and a possible deformation of GNRs from rod-like to sphere. After 3 repeated irradiation processes, the LSPR peaks nearly vanished.

In the case of GO-GNRs, a typical GO band was observed around 230nm, which indicated that GNRs were successfully incorporated with GO nanosheets in ammonium hydroxide. On the contrary to the dramatic spectral changes of CTAB-GNR samples, no amplitude diminishment of the LSPR peak with a slight blue-shift (up to 8 nm) was observed for GO-GNR nanocomposites when irradiated under the same experimental conditions (Figure 6, B, D, F). Such slight blue-shift did not affect the availability and property of those nanocomposites, which has already been confirmed in the photothermal experiments mentioned above. The high reproducibility in the UV-visible spectra firmly demonstrated both shape stability and colloid stability of these GO-GNR nanocomposites under considerable NIR irradiation.

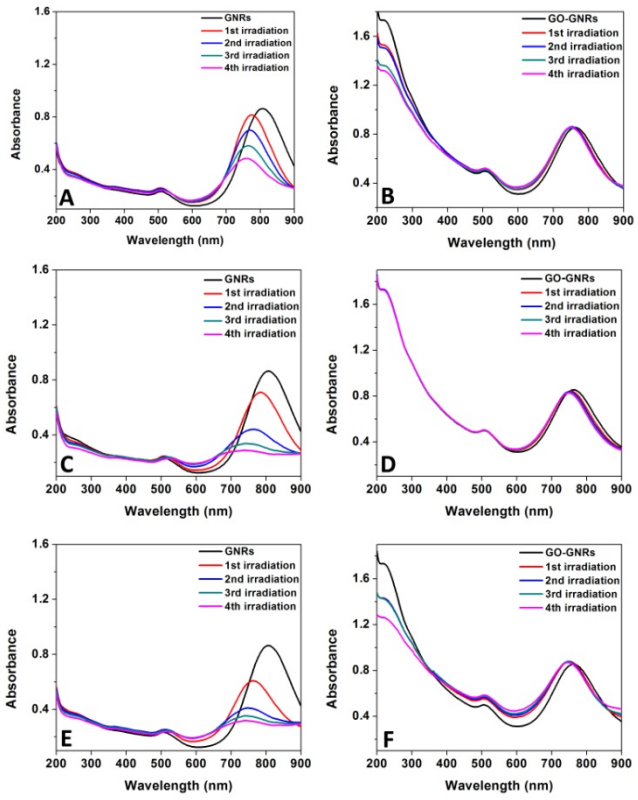

Figure 6. UV-visible spectra of CTAB-GNRs (A, C, E) and GO-GNR (B, D, F) solutions after repeated laser radiation at different laser intensities (A, B: 1.5 W/cm^2; C, D: 1.9 W/cm^2; E, F: 2.3 W/cm^2).

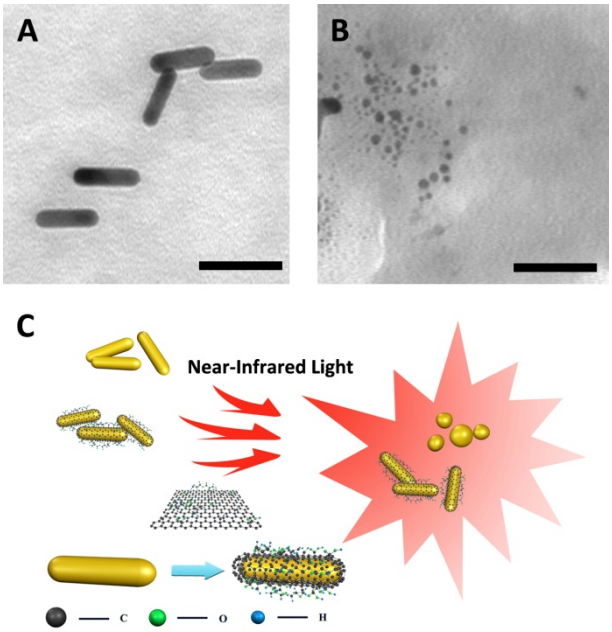

Figure 7. TEM images of the laser-irradiated GO-GNRs (A) and CTAB-GNRs (B). (Scale bars: 50 nm) (C) Schematic illustration of the difference in Photothermal stability between CTAB-GNRs and GO-GNRs

The photothermal stability of GO-GNR nanocomposites was further confirmed by TEM characterization. No distinct change was found for GO-GNR after 4 repeated NIR irradiation at 2.3W/cm^2 (Figure 7A). However, for CTAB-GNRs, irradiation under the same condition resulted in a dramatic reshaping from nanorods into typical spherical and amorphous nanoparticles for most of GNRs (Figure 7B). The observed poor shape stability of CTAB-GNRs was consistent with the significant spectral changes we discussed above.

Figure 7C vividly illustrated the difference in photothermal stability between CTAB-GNRs and GO-GNRs. Our results indicated that enhanced photothermal stability of GNRs can be achieved through being wrapped by a thin layer of GO nanosheet. In this laser induced heating, heat is generated directly from the NIR-responsive GNRs, which leads to great temperature gradients. Melting of GNRs could be ascribed to the high lattice temperature on GNR surface, which is much higher than the detected temperature of the solution. The thermal conductivity of the coating layer is very crucial for the reshaping of GNRs in solution[13, 31]. With a higher thermal conductivity, the heat can release faster from GNR surface, and as a consequence, the lattice temperature could be lower, which benefits the shape stability of GNRs. GO has a much higher thermal conductivity compared with water[32], which might be the reason for the enhanced photothermal stability of GO-GNRs.

Previously, enhance photothermal stability has been reported for GNRs with silica coating[16] or polyelectrolyte encapsulation[17]. Our GO-GNRs nanocomposite appears to be more biocompatible with an excellent reproducibility of photothermal performance.

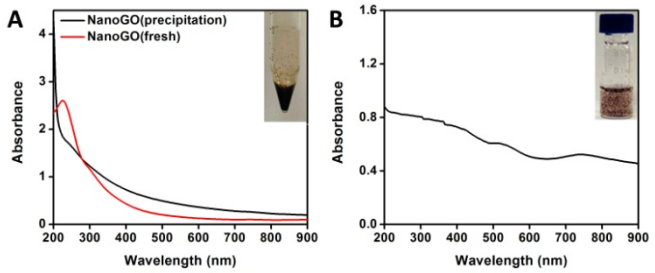

Figure 8. (A) UV-visible spectra of the fresh nanoGO (red line) and the nanoGO after one week storage at room temperature (black line). Insert: Photo image of the nanoGO sample after one week storage. (B) UV-visible spectra of GO-GNRs complex synthesized through a rapid mixing method. Insert: Photo image of that coalescence.

In addition, we found that if not incorporated with GNRs, the exfoliated nanoGO in ammonium hydroxide solution showed distinguish aggregation after one week of storage (Figure 8A, insert). The aggregation of nanoGO could be further confirmed by the vanished peak at 270nm in the UV-visible spectra (Figure 8A). On the contrary, no sedimentation was found for the GO-GNR nanocomposites after a few weeks, which showed adequate colloidal stability of the sample.

It should be noted that, the way how to mix sample solutions is very crucial. Good colloidal stability could only be obtained when GNRs solution was added into nanoGO solution in a dropwise manner. Otherwise, immediate coalescence of nanoparticles occurred when quick mixing of these two solutions (Figure 8B, inserted), which has been previously reported[22]. As shown in UV-vis spectra, the intensity of LSPR band at 780 nm almost disappeared, which further confirmed the coalescence of the GNRs. Apparently, in the case of coalescence, rather than providing additional protection for GNRs, the negative charged GO nanosheets might induce desorption of the positively charged CTAB bilayer from GNRs surface through a strong electrostatic interaction. Disruption of the protective CTAB bilayer on GNRs surface would eventually facilitate the reshaping of GNRs[33]. Therefore, we proposed that the enhanced photothermal stability and prolonged photothermal performance can only be achieved when individual GNR was well wrapped by nanoGO sheets.

Conclusions

In summary, NIR-sensitive photothermal nanocomposites of nanosized GO and plasmonic GNRs were fabricated. In comparison to the as-synthesized CTAB-GNRs, the nanoGO wrapped GNRs showed enhanced morphological stability and high reproducibility in photothermal performance under NIR irradiation. This is a significant breakthrough of conquering laser-induced melting of anisotropic gold nanoparticles. Based on the greatly enhanced photothermal stability of GNRs, our results may be useful in improving the diagnosis and treatment efficiency of photothermal therapy. In addition, these nanoscaled structures will be promising for further encapsulation inside some drug-delivery carriers with proper biocompatibility such as liposome[34] and polymers.

Acknowledgements

This work was financially supported by the NSFC (No. 21203128), the General Program of Science and Technology Development Project of Beijing Municipal Education Commission of China (KM201310028006), and The Project of Construction of Innovative Teams and Teacher Career Development for Universities and Colleges under Beijing Municipality (IDHT20140512).

References

1. C. Bao, N. Beziere, P. del Pino, B. Pelaz, G. Estrada, F. Tian, [illegible] Ntziachristos, J. M. de la Fuente and D. Cui, *Small*, 2013, [illegible] 68-74.
2. P. Vijayaraghavan, C. H. Liu, R. Vankayala, C. S. Chiang and K. [illegible] Hwang, *Advanced Materials*, 2014, **26**, 6689-6695.
3. C. M. Hessel, V. P. Pattani, M. Rasch, M. G. Panthani, B. Koo, J. W. Tunnell and B. A. Korgel, *Nano letters*, 2011, **11**, 2560-2566.
4. J. Shi, L. Wang, J. Zhang, R. Ma, J. Gao, Y. Liu, C. Zhang and Z. Zhang, *Biomaterials*, 2014, **35**, 5847-5861.
5. C. Ayala-Orozco, C. Urban, M. W. Knight, A. S. Urban, O. Neumann, S. W. Bishnoi, S. Mukherjee, A. M. Goodman, H. Charron and T. Mitchell, *ACS nano*, 2014, **8**, 6372-6381.
6. N. Nath and A. Chilkoti, *Analytical Chemistry*, 2002, **74**, 504-509.
7. B. Nikoobakht and M. A. El-Sayed, *Chemistry of Materials*, 2003, **15**, 1957-1962.
8. A. Agarwal, M. A. Mackey, M. A. El-Sayed and R. V. Bellamkonda, *ACS nano*, 2011, **5**, 4919-4926.
9. E. E. Connor, J. Mwamuka, A. Gole, C. J. Murphy and M. D. Wyatt, *Small*, 2005, **1**, 325-327.
10. Q. Dai, J. Coutts, J. Zou and Q. Huo, *Chem. Commun.*, 2008, 2858-2860.
11. C. Li, C. Qiu, Y. Zhang and D. Li, *Materials Letters*, 2015, **140**, 184-186.
12. T. S. Hauck, A. A. Ghazani and W. C. Chan, *Small*, 2008, **4**, 153-159.
13. Y. Horiguchi, K. Honda, Y. Kato, N. Nakashima and Y. Niidome, *Langmuir*, 2008, **24**, 12026-12031.
14. S. Link, C. Burda, M. Mohamed, B. Nikoobakht and M. El-Sayed, *The Journal of Physical Chemistry A*, 1999, **103**, 1165-1170.
15. H. Petrova, J. Perez Juste, I. Pastoriza-Santos, G. V. Hartland, L. M. Liz-Marzan and P. Mulvaney, *Physical Chemistry Chemical Physics*, 2006, **8**, 814-821.
16. Y. S. Chen, W. Frey, S. Kim, K. Homan, P. Kruizinga, [illegible] Sokolov, S. Emelianov, *Optics express*, 2010, **18**, 8867-8878.
17. H. C. Huang, S. Barua, D. B. Kay and K. Reg, *ACS Nano*, 2009, **3**, 2941-2952.
18. J. Pyun, *Angewandte Chemie International Edition*, 2011, **50**, 46-48.

19. L. Wang, K. Lee, Y.-Y. Sun, M. Lucking, Z. Chen, J. J. Zhao and S. B. Zhang, *ACS nano*, 2009, **3**, 2995-3000.
20. X. Sun, Z. Liu, K. Welsher, J. T. Robinson, A. Goodwin, S. Zaric and H. Dai, *Nano research*, 2008, **1**, 203-212.
21. Y. Chang, S.-T. Yang, J.-H. Liu, E. Dong, Y. Wang, A. Cao, Y. Liu and H. Wang, *Toxicology letters*, 2011, **200**, 201-210.
22. C. Hu, J. Rong, J. Cui, Y. Yang, L. Yang, Y. Wang and Y. Liu, *Carbon*, 2013, **51**, 255-264.
23. D.-K. Lim, A. Barhoumi, R. G. Wylie, G. Reznor, R. S. Langer and D. S. Kohane, *Nano letters*, 2013, **13**, 4075-4079.
24. C. J. Orendorff, and C. J. Murphy, The Journal of Physical Chemistry B, 2006, **110**, 3990-3994.
25. J. Zhou, Z. Lu, X. Zhu, X. Wang, Y. Liao, Z. Ma and F. Li, *Biomaterials*, 2013, **34**, 9584-9592.
26. H. Kinoshita, Y. Nishina, A. A. Alias and M. Fujii, *Carbon*, 2014, **66**, 720-723.
27. X. Li, H. Zhou, W. Wu, S. Wei, Y. Xu and Y. Kuang, *Journal of colloid and interface science*, 2015, **448**, 389-397.
28. I. K. Moon, J. Lee, R. S. Ruoff and H. Lee, *Nature communications*, 2010, **1**, 73.
29. J. Yu, J. Jin, B. Cheng and M. Jaroniec, *Journal of Materials Chemistry A*, 2014, **2**, 3407-3416.
30. B. Konkena and S. Vasudevan, *The Journal of Physical Chemistry Letters*, 2012, **3**, 867-872.
31. J. Huang, J. Park, W. Wang, C. J. Murphy and D. G. Cahill, *ACS nano*, 2013, **7**, 589-597.
32. H. Im, J. Kim, *Carbon*, 2012, **50**, 5429-5440.
33. H. Pan, S. Low, N. Weerasuriya and Y.-S. Shon, *ACS applied materials & interfaces*, 2015, 7, 3406-3413.
34. M. M. van Schooneveld, E. Vucic, R. Koole, Y. Zhou, J. Stocks, D. P. Cormode, C. Y. Tang, R. E. Gordon, K. Nicolay and A. Meijerink, *Nano letters*, 2008, **8**, 2517-2525.